TIDAL SIGNALS IN GOCE MEASUREMENTS AND TIME-GCM

K. Häusler[1], M. E. Hagan[1], G. Lu[1], E. Doornbos[2], S. Bruinsma[3], and J. M. Forbes[4]

[1]*High Altitude Observatory, National Center for Atmospheric Research, P.O. Box 3000, Boulder, CO 80307-3000, USA (kathrin@ucar.edu, hagan@ucar.edu, ganglu@ucar.edu)*

[2]*Delft University of Technology, Aerospace Engineering, Kluyverweg 1, 2629 HS Delft, The Netherlands (e.n.doornbos@tudelft.nl)*

[3]*Department of Terrestrial and Planetary Geodesy, CNES, 18 avenue E. Belin, 31401 Toulouse Cedex 9, France (sean.bruinsma@cnes.fr)*

[4]*Aerospace Engineering Sciences ECOT-634, University of Colorado UCB429, Boulder, CO 80309, USA (forbes@colorado.edu)*

ABSTRACT

In this paper we investigate tidal signatures in GOCE measurements during 15-24 November 2009 and complementary simulations with the Thermosphere-Ionosphere-Mesosphere-Electrodynamics General Circulation Model (TIME-GCM). The TIME-GCM simulations are driven by inputs that represent the prevailing solar and geomagnetic conditions along with tidal and planetary waves applied at the lower boundary (ca. 30km). For this pilot study, the resultant TIME-GCM densities are analyzed in two ways: 1) we use results along the GOCE orbital track, to calculate ascending/descending orbit longitude-latitude density difference and sum maps for direct comparison with the GOCE diagnostics, and 2) we conduct a complete analysis of TIME-GCM results to unambiguously characterize the simulated atmospheric tides and to attribute the observed longitude variations to specific tidal components. TIME-GCM captures some but not all of the observed longitudinal variability. The good data-model agreement for wave-2, wave-3, and wave-4 suggests that thermospheric impacts can be attributed to the DE1, DE2, DE3, S0, SE1, and SE2 tides. Discrepancies between TIME-GCM and GOCE results are most prominent in the wave-1 variations, and suggest that further refinement of the lower boundary forcing is necessary before we extend our analysis and interpretation to densities associated with the remainder of the GOCE mission.

1. INTRODUCTION

Numerous observations and model studies made during the past years have unequivocally revealed that geospace owes a considerable amount of its longitudinal, local time, seasonal/latitudinal and day-to-day variability to solar atmospheric tides that propagate upward from the lower atmosphere. Solar atmospheric tides are global scale waves in all atmospheric fields, including temperature, density, and wind. They are generated by the energy input of the Sun into Earth's atmosphere and are therefore characterized by periods that are harmonics of a day. The parts of the tidal spectrum that follow the apparent westward propagation of the Sun from the perspective of a ground-based observer are called migrating tides, and the non-Sun-synchronous parts are called nonmigrating tides [e.g., 1, 2]. Nonmigrating tides can either propagate eastward (E), westward (W) or remain standing with the longitudinal variation (i.e., number of maxima/minima) given by zonal wavenumber *s*. Diurnal (D) oscillations have a period of 24 hours while semidiurnal (S) oscillations have a period of 12 hours. It is the upward propagating nonmigrating components that have demonstrated the most significant impact on the ionosphere-thermosphere system and are the focus of our study. Throughout this paper we will use the letter/number combination *DWs (SWs)* and *DEs (SEs)*) to respectively describe a westward or eastward propagating diurnal (semidiurnal) tide with zonal wavenumber *s*. Standing tidal oscillations exhibit no longitudinal variability and are termed *D0* and *S0*. Stationary planetary waves have no periodicity; their longitudinal variability is characterized by zonal wavenumber *m*, and they are labeled as *sPWm*.

Examples of nonmigrating tides present in the mesosphere and lower thermosphere (MLT) region can be found in [3], wherein the authors present tidal signatures derived from TIMED (Thermosphere Ionosphere Mesosphere Energetics and Dynamics) SABER (Sounding of the Atmosphere using Broadband Emission Radiometry) temperature measurements. Among the most prominent tide in the MLT region is the diurnal eastward propagating tide with zonal wavenumber three (DE3) which is excited by latent heat release in the tropics. The DE3 tide is also found in CHAMP (Challenging Minisatellite Payload) satellite measurements at approximately 400 km altitude, which demonstrates the unanticipated vertical coupling from the tropical troposphere to the upper thermosphere. An overview of CHAMP tides can be found in [4] and [5]. The CHAMP mission ended September 2010 with the reentry of the satellite into the atmosphere but another ongoing satellite mission is GRACE (Gravity Recovery And Climate Experiment). Like CHAMP, GRACE has an accelerometer onboard measuring the

Proc. 'ESA Living Planet Symposium 2013', Edinburgh, UK 9–13 September 2013 (ESA SP-722, December 2013)

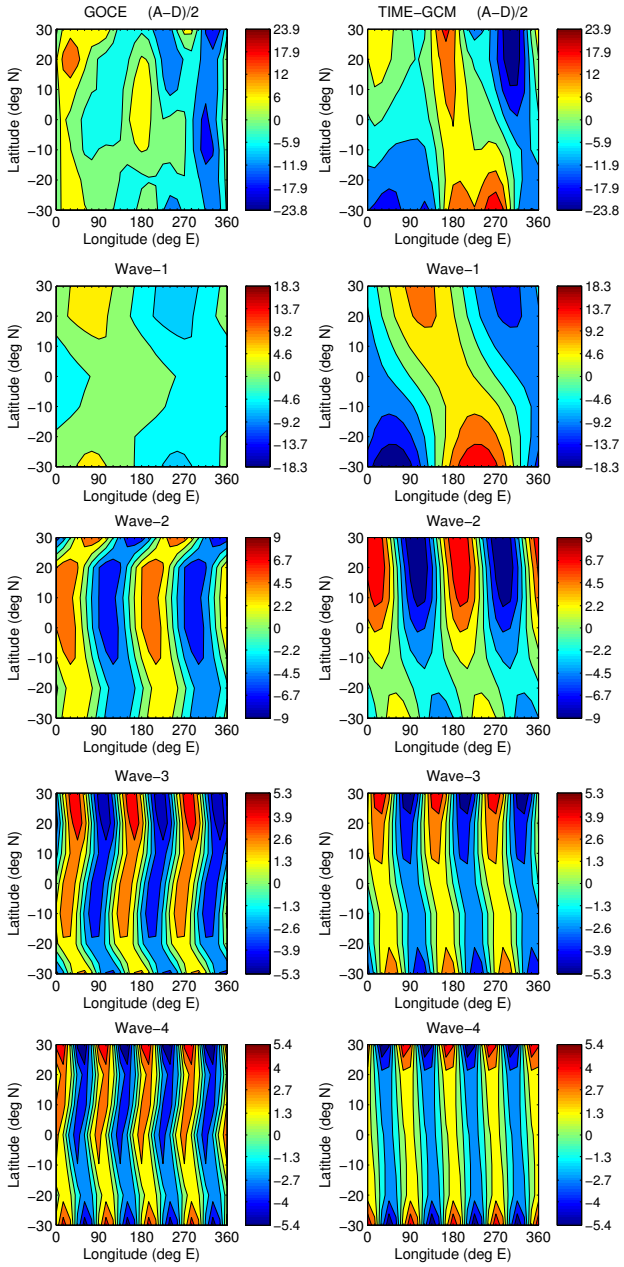

Figure 1. Neutral density ($10^{-13} kg/m^3$) orbital differences (a-d)/2 for GOCE (left panels) and TIME-GCM (right panels). Top panels are the combined wave-1,2,3,4 signals from the least square fitting procedure, while the following panels from row 2 to row 5 are the single wave-1,2,3,4 components, respectively.

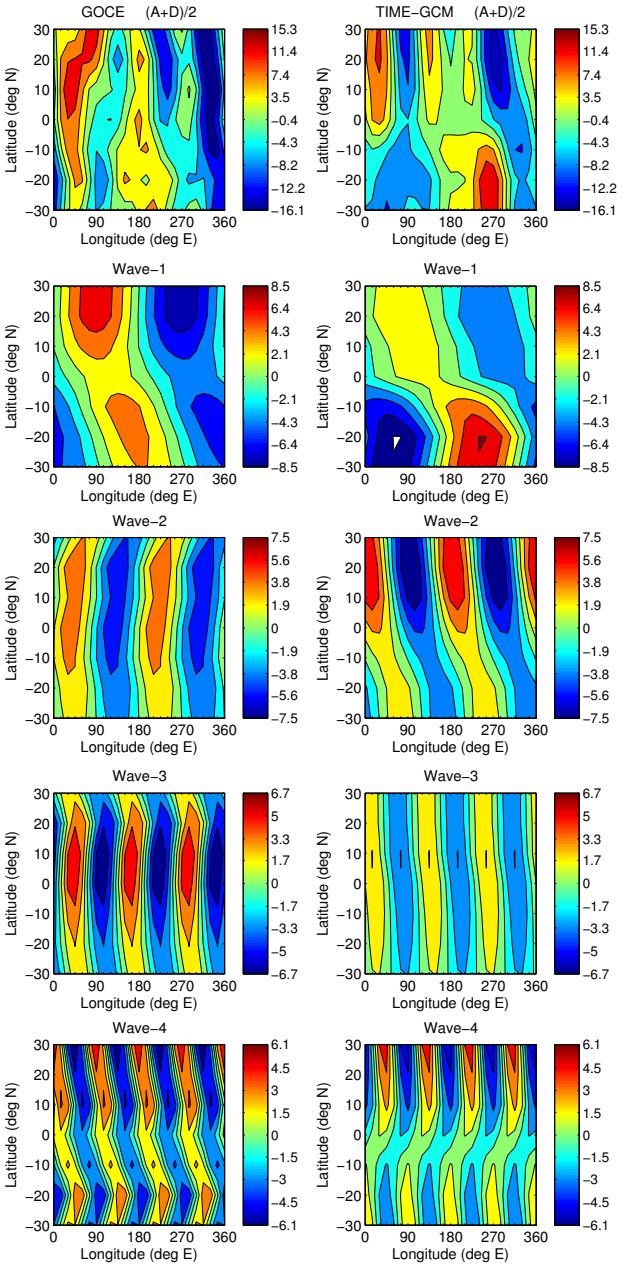

Figure 2. Same as Fig. 1 but for the orbital sums (a+d)/2.

neutral density at orbit altitude. CHAMP and GRACE measurements have also been combined to quantify thermospheric tidal signatures attributable to DE3 and other important nonmigrating components [6, 7].

The GOCE satellite was launched 17 March 2009 into a Sun-synchronous orbit with an inclination of 96.7°. The satellite carries six accelerometers as part of its gravity gradiometer instrument measuring the neutral density and zonal wind at approximately 270 km altitude. The algorithm for the density and wind determination is described in [8]. The GOCE altitude region complements measurements made by the CHAMP, GRACE, and TIMED satellite, thus filling the long-standing middle thermosphere measurement gap. However, the characteristic Sun-synchronous orbit distinguishes GOCE from the CHAMP and GRACE satellites and presents a challenge for tidal analysis due to limited local time coverage. In the case of the GOCE orbit where only two local times are available, we employ a technique previously demonstrated by [7] to quantify thermospheric longitudinal variability that can be attributed to nonmigrating tides and stationary planetary waves. Specifically, we calculate longitude-latitude difference and sum maps of density us-

Table 1. The listed diurnal (D) and semidiurnal (S) oscillations propagating either eastward (E) or westward (W) with a given zonal wavenumber, s, or standing (0) as well as stationary planetary waves (sPWm) can account for the observed wave - m structures in satellite data taken at quasi-constant local time.

OBSERVED	ACCOUNTING OSCILLATIONS				
wave - 1	DW2,	D0,	SW3,	SW1,	sPW1
wave - 2	DW3,	DE1,	SW4,	S0,	sPW2
wave - 3	DW4,	DE2,	SW5,	SE1,	sPW3
wave - 4	DW5,	DE3,	SW6,	SE2,	sPW4

ing the ascending (a) and descending (d) portions of the GOCE orbit to separate variations attributable to the diurnal ($(a-d)/2$) and semidiurnal ($(a+d)/2$) tides, as well as stationary planetary waves. Since more than one tidal component can give rise to the same longitudinal structure (cf. Tab. 1), we invoke a model to help identify the observed tidal signals. Concurrently, we use the unique perspective of the middle thermosphere GOCE observations to further validate our model.

In this paper we present longitudinal variations observed by the GOCE satellite and compare them with the results of TIME-GCM, which is used to identify the prevailing tidal signals that are causing the observed longitudinal variations in GOCE. The following section describes the TIME-GCM in more detail along with some more specifics of our orbital analysis technique. Section 3 contains the results while Section 4 provides a discussion and a summary.

2. MODEL AND DATA ANALYSIS

The TIME-GCM is a three-dimensional time-dependent global grid point model that calculates the dynamics, electrodynamics, energetics, and the compositional structure of the middle and upper atmosphere from first principles. A more complete description of the model, which was developed at the National Center for Atmospheric Research, is given by [9–11] and references therein. TIME-GCM is able to inherently calculate the atmospheric tides that are excited by the absorption of ultraviolet and extreme ultraviolet radiation in the middle and upper atmosphere. Nevertheless, TIME-GCM cannot account for tidal components that are excited by latent heat release in deep tropical clouds or by the absorption of infrared radiation [12]. In order to introduce the tides of tropospheric origin into the TIME-GCM, the lower boundary (i.e., 10 mb; $\sim$30 km) is driven by climatological tidal results from the global scale wave model (GSWM) [e.g., 13, 14]. The GSWM was recently updated with new tidal heating rates using International Satellite Cloud Climatology Project (ISCCP) radiative fluxes and Tropical Rainfall Measuring Mission (TRMM) latent heating profiles and TRMM rainfall rates [3, 15].

For the simulation discussed herein, we ran the TIME-GCM with 2.5° by 2.5° horizontal resolution and 4 grid points per scale height in the vertical for the time period 15-24 Nov 2009. We also introduced daily-averaged ECMWF (European Centre for Medium-Range Weather Forecasts) data at the lower boundary to account for day-to-day variations, including planetary wave activity. The aforementioned GSWM lower boundary forcing includes westward propagating zonal wavenumber 6 (W6) through eastward propagating zonal wavenumber 6 (E6) diurnal and semidiurnal components. We analyzed the model in two ways. First, the TIME-GCM thermospheric densities were sampled along the GOCE orbit thus creating a set of TIME-GCM densities that identically complement the GOCE data. For each day between 15-24 November 2009 and for both GOCE and TIME-GCM, we calculated longitude-latitude thermospheric density maps from ascending and descending orbit differences and sums as described in the introduction. We restricted our analysis to $\pm 35^\circ$ in 10° steps where we expect the impacts of the upward propagating nonmigrating tides to be most prominent. For each latitude bin we than decomposed the longitudinal variations into the wave-1, through wave-4 components, using a least-square fitting method to the average in each latitude bin over the ten-day period.

We also analyzed the entire set of hourly TIME-GCM density results at 270 km for the ten-day simulation period by fitting them at each latitude using a regression analysis of the form:

$$\Sigma A_{n,s} cos(n\Omega(t_{UT}) + s\lambda - \phi_{n,s}) \qquad (1)$$

where A_{ns} is the amplitude of the *n*th tidal harmonic with zonal wavenumber s, Ω is the Earths rotation rate (i.e., 2π/24 hours), t_{UT} is universal time in hours, and $\phi_{n,s}$ is the tidal phase (i.e., the universal time of maximum at 0° longitude). The resultant tidal amplitudes and phases unambiguously characterize the simulated atmospheric tidal components.

3. RESULTS

Neutral density ten-day mean orbit difference least square fits for the time period 15-24 November 2009 are presented in Fig. 1. The difference fields are mostly attributable to the nonmigrating diurnal tides. The left panels show GOCE results while the right panels depict TIME-GCM simulations sampled along the GOCE orbit. The two top panels show a combination of the observed wave-1,2,3,4 longitudinal structures while the following panels show the contributing wave-1 through wave-4 components. The top two panels reveal that TIME-GCM captures some salient observational features in the northern tropics but there is little agreement between GOCE and TIME-GCM in the southern tropics. The wave-1 component predicted by TIME-GCM is almost three times stronger than the one observed by GOCE and it is also shifted in longitude in the southern tropics. The maximum of the GOCE wave-1 structure shown for the latitudinal range of $\pm 30^\circ$ is reached at 75°E longitude with an amplitude of $6.4 \times 10^{-13} kg/m^3$ at 30°N while the TIME-GCM wave-1 maximizes at 225°E longitude with an amplitude of $18.3 \times 10^{-13} kg/m^3$ at 30°S. For the wave-2 component we find good agreement near the equator between the two data sets but again the maxi-

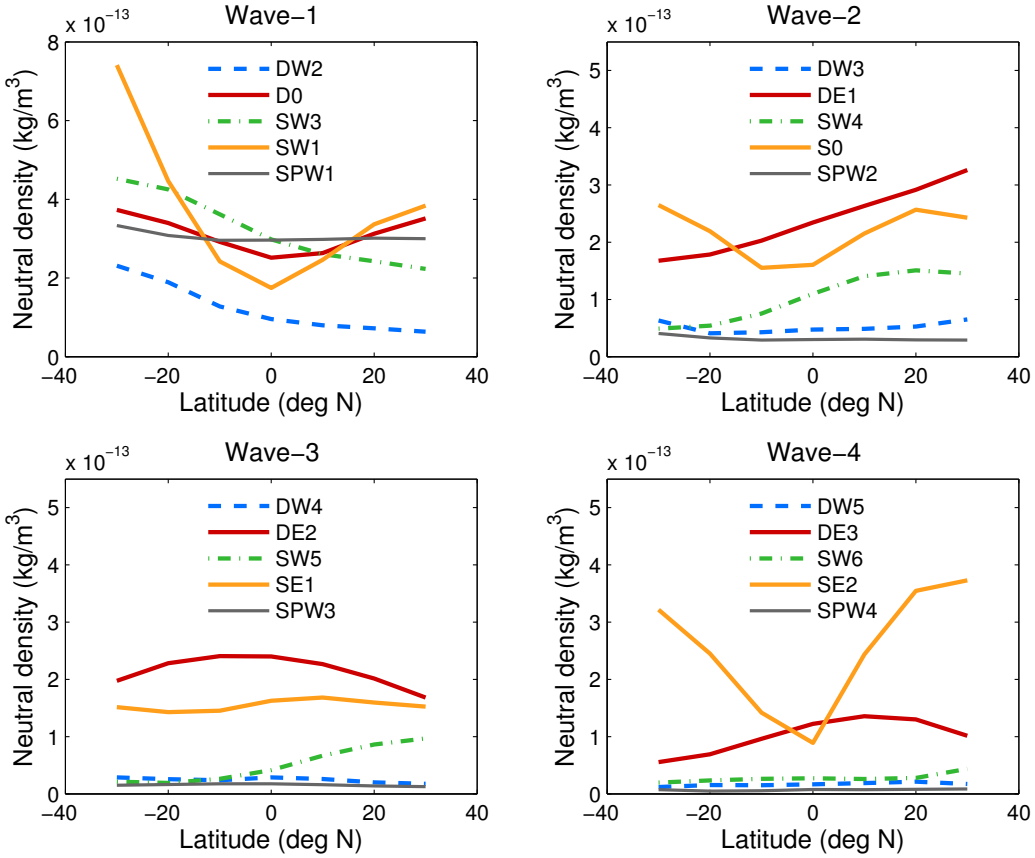

Figure 3. Neutral density TIME-GCM tidal diagnostics for the time period 15-24 November 2009. Indicated on top of each panel are the corresponding observed wavenumbers in the satellite perspective (see Tab. 1).

mum amplitude is found for TIME-GCM this time in the northern hemisphere amounting to $9.0 \times 10^{-13} kg/m^3$ at 15°E and 195°E longitude compared to GOCE with $6.6 \times 10^{-13} kg/m^3$ at 75°E and 255°E longitude. The wave-3 and wave-4 structures exhibit very good agreement at 30°N and 30°S. The maximum amplitudes are almost the same between the two data sets and found at 30°N. For GOCE they are $4.8 \times 10^{-13} kg/m^3$ (wave-3) and $5.4 \times 10^{-13} kg/m^3$ (wave-4). For TIME-GCM they are both $5.3 \times 10^{-13} kg/m^3$. The location of the maxima between GOCE and TIME-GCM is shifted by 15° in longitude for the wave-3 while it is shifted by 30° in longitude for the wave-4, and TIME-GCM exhibits weaker amplitudes in the equatorial region in both of these wave components.

Fig. 2 is structured the same way as Fig. 1 except the orbit sums, which are mostly attributable to the nonmigrating semidiurnal tides and stationary planetary waves, are shown. The orbital sum field is comparatively smaller than the orbital difference field shown in Fig. 1. Similar to the orbital difference field, the comparison between GOCE and TIME-GCM for the wave-1 component is poor, especially in the southern region. The maximum wave-1 amplitude for TIME-GCM is found at 20°S and 240°E amounting to $8.5 \times 10^{-13} kg/m^3$ while the maximum amplitude of GOCE in the southern hemisphere is found at 10°S and 150°E amounting to $5.3 \times 10^{-13} kg/m^3$. The peak wave-1 amplitude of $7.7 \times 10^{-13} kg/m^3$ for GOCE is found in the northern hemisphere at 30°N and 90°E. For this location TIME-GCM predicts an amplitude of only $2.9 \times 10^{-13} kg/m^3$ but GOCE and TIME-GCM are at least in phase in the northern hemisphere. TIME-GCM slightly overestimates the wave-2 component but largely captures the longitudinal distribution with a slight longitudinal shift that isn't present in the GOCE observations. While TIME-GCM peaks with $7.5 \times 10^{-13} kg/m^3$ at 20°N and 0°E and 180°E longitude, GOCE peak amplitudes of $5.5 \times 10^{-13} kg/m^3$ are reached at 20°N and 45°E and 225°E longitude. However, the agreement in the southern hemisphere is much better where TIME-GCM peaks with an amplitude of $3.3 \times 10^{-13} kg/m^3$ compared to $2.9 \times 10^{-13} kg/m^3$ for GOCE, and the longitudinal shift between the two data sets only amounts to 30°. TIME-GCM captures the orbital sum field for the wave-3 component quite well with only a slight longitudinal shift of 30° but the amplitudes are mostly only half or less of the observed GOCE amplitudes. The amplitude agreement between GOCE and TIME-GCM is much better for the wave-4 structure especially in the nothern hemisphere and the equatorial region. Peak amplitudes for GOCE and TIME-GCM are $6.1 \times 10^{-13} kg/m^3$ and $5.1 \times 10^{-13} kg/m^3$, respectively, at 30°N and the longitudinal shift is 45°.

The advantage of the model is that it provides hourly and globally distributed data output for every single day, which allows us to unambiguously calculate the TIME-GCM ten-day average tidal spectrum (Eq. 1). The tidal components, which can account for the observed wave structures in satellite data (see Tab. 1) are depicted in Fig. 3. They are also ten-day averages for the period 15-24 November 2009. We can use these results to attribute the prominent tidal oscillation to the calculated TIME-GCM wave structures along the GOCE orbit shown in Fig. 1 and Fig. 2. Where the GOCE and TIME-GCM results are comparable, we can extend the attribution to the observed longitudinal variability. SE2 clearly dominates the wave-4 structure and is most likely responsible for the observed wave-4 structure in GOCE with a secondary DE3 contribution. The observed wave-2 and wave-3 structures are likely attributable to the combination of DE1 and S0 and DE2 and SE1, respectively, with smaller SW4 and SW5 contributions in the northern hemisphere. The TIME-GCM wave-1 structure is attributable to a combination of all candidate tidal components, but because the agreement between GOCE and TIME-GCM is very poor we cannot attribute the TIME-GCM results to the observed wave-1 structure in GOCE.

4. DISCUSSION AND SUMMARY

In this paper we presented GOCE and TIME-GCM thermospheric density orbital analyses for a ten-day solar minimum and geomagnetically quiescent period in November 2009. The model-measurement comparisons reveal both similarities and differences. The differences between GOCE and TIME-GCM may be partially attributable to shortcomings in the lower boundary forcing in TIME-GCM due to meteorological variability that cannot be captured by the climatological tidal forcing that characterized our numerical simulation. To address this shortcoming and to improve the predictive capabilities of the model, we will use MERRA (Modern-era Retrospective Analysis for Research and Application) reanalysis data as a lower boundary forcing in our follow-on TIME-GCM simulations.

In spite of the aforementioned shortcoming, our results demonstrate that in cases where GOCE and TIME-GCM agree very well, the full model wave analyses allows us to interpret the observed GOCE longitudinal variability. For example, we demonstrated that nonmigrating tides are primarily responsible for the observed wave-2, wave-3, and wave-4 GOCE density perturbations. The strongest among them are DE1, S0, DE2, SE1, and SE2 for the time period 15-24 November 2009. Given this demonstrated capability, we plan to extend our analyses to other time periods and to investigate tidal signatures in thermospheric zonal winds in addition to densities. These efforts will serve to further evaluate TIME-GCM and aid the interpretation of GOCE tidal diagnostics.

ACKNOWLEDGMENTS

This work was supported in part by the NASA USPI-GOCE award. The production of GOCE thermosphere density data products is supported by the ESA Support To Science Element program. KH is supported by the Advanced Study Program Postdoctoral Fellowship of the National Center for Atmospheric Research. The National Center for Atmospheric Research is sponsored by the National Science Foundation.

REFERENCES

1. Chapman, S. & Lindzen, R.S. (1970). *Atmospheric Tides: Thermal and Gravitational*. D. Reidel Publishing Company, Dordrecht, Holland.

2. Forbes, J.M. (1995). Tidal and Planetary Waves. R.M. Johnson & T.L. Killeen, (eds.) *The Upper Mesosphere and Lower Thermosphere: A Review of Experiment and Theory*, *Geophys. Monogr. Ser.*, vol. 87, AGU, Washington, DC.

3. Zhang, X., Forbes, J.M. & Hagan, M.E. (2010). Longitudinal variation of tides in the MLT region: 1. Tides driven by tropospheric net radiative heating. *J. Geophys. Res.*, 115, A06 316.

4. Häusler, K. & Lühr, H. (2009). Nonmigrating tidal signals in the upper thermospheric zonal wind at equatorial latitudes as observed by CHAMP. *Ann. Geophys.*, 27, 2643–2652.

5. Lieberman, R.S., Akmaev, R.A., Fuller-Rowell, T.J. & Doornbos, E. (2013). Thermospheric zonal mean wind and tides revealed by CHAMP. *Geophys. Res. Lett.*, 40, 2439–2443.

6. Forbes, J.M., Bruinsma, S.L., Zhang, X. & Oberheide, J. (2009). Surface-exosphere coupling due to thermal tides. *Geophys. Res. Lett.*, 36, L15 812.

7. Forbes, J.M., Zhang, X. & Bruinsma, S. (2012). Middle and upper thermosphere density structures due to nonmigrating tides. *J. Geophys. Res.*, 117, A11 306.

8. Doornbos, E., van den IJssel, J., Lühr, H., Förster, M. & Koppenwallner, G. (2010). Neutral density and crosswind determination from arbitrarily oriented multiaxis accelerometers on satellites. *J. Spacecraft Rockets*, 47(4), 580–589.

9. Roble, R.G. (1995). Energetics of the mesosphere and thermosphere. R.M. Johnson & T.L. Killeen, (eds.) *The Upper Mesosphere and Lower Thermosphere: A Review of Experiment and Theory*, *Geophys. Monogr. Ser.*, vol. 87, 1–21, AGU, Washington, DC.

10. Roble, R.G. (1996). The NCAR thermosphere-ionosphere-mesosphere-electrodynamics general circulation model (TIME-GCM). R.W. Schunk, (ed.) *STEP Handbook on Ionospheric Models*, 281–288, Utah State University, Logan.

11. Roble, R.G. & Ridley, E.C. (1994). A thermosphere-ionosphere-mesosphere-electrodynamics general circulation model (time-GCM): Equinox solar cycle minimum simulations (30-500 km). *Geophys. Res. Lett.*, 21, 417–420.

12. Hagan, M.E., Maute, A., Roble, R.G., Richmond, A.D., Immel, T.J. & England, S.L. (2007). Connections between deep tropical clouds and the Earth's ionosphere. *Geophys. Res. Lett.*, 34, L20 109.

13. Hagan, M.E. & Forbes, J.M. (2002). Migrating and nonmigrating diurnal tides in the middle and upper atmosphere excited by tropospheric latent heat release. *J. Geophys. Res.*, 107(D24), 4754.

14. Hagan, M.E. & Forbes, J.M. (2003). Migrating and nonmigrating semidiurnal tides in the upper atmosphere excited by tropospheric latent heat release. *J. Geophys. Res.*, 108(A2), 1062.

15. Zhang, X., Forbes, J.M. & Hagan, M.E. (2010). Longitudinal variation of tides in the MLT region: 2. Relative effects of solar radiative and latent heating. *J. Geophys. Res.*, 115, A06 317.